Electronic Supplementary Material (ESI) for RSC Advances.

Supplementary Information

MOF-derived Manganese Oxide/Carbon Nanocomposites with Raised Capacitance for Stable Asymmetric Supercapacitor

By Ruoyu Wang, Yating Hu, Zhenghui Pan, John Wang,**

Email: msepz@nus.edu.sg; msewangj@nus.edu.sg

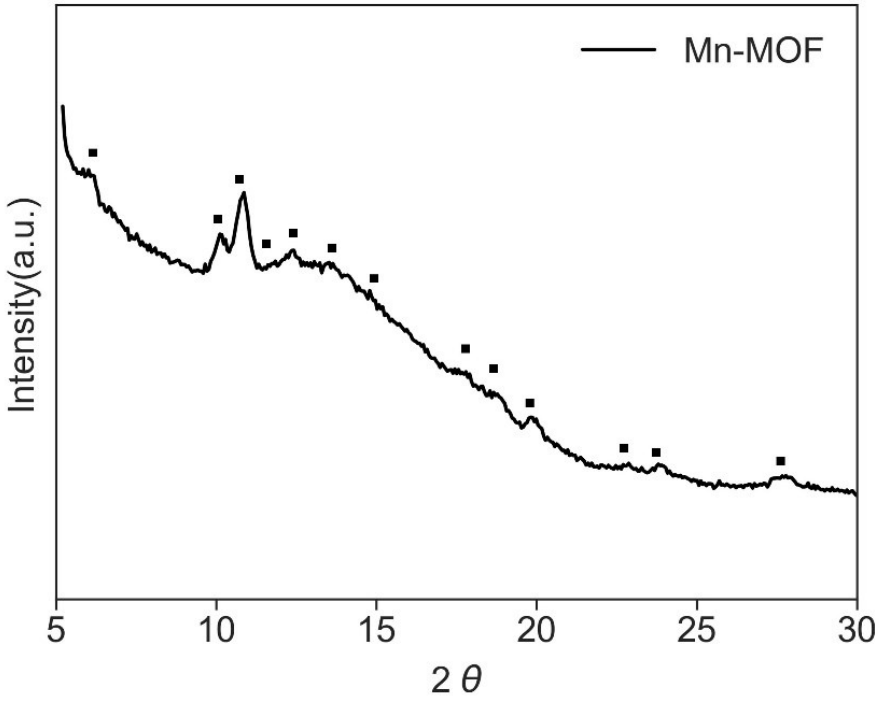

Figure S1. The XRD of as synthesized Mn-MIL-100.

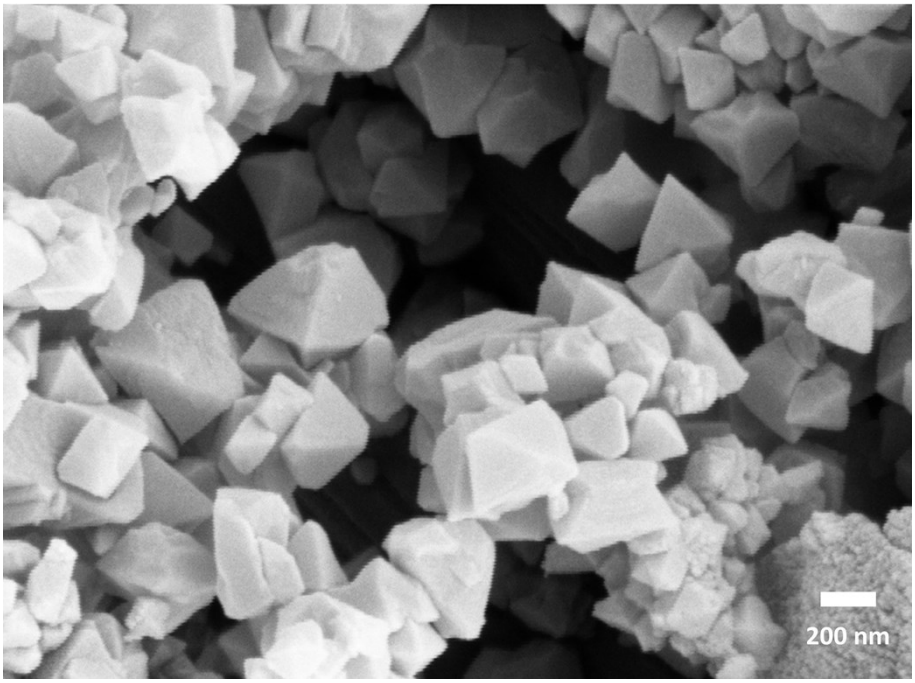

Figure S2. The SEM image of Mn-MIL-100 MOF.

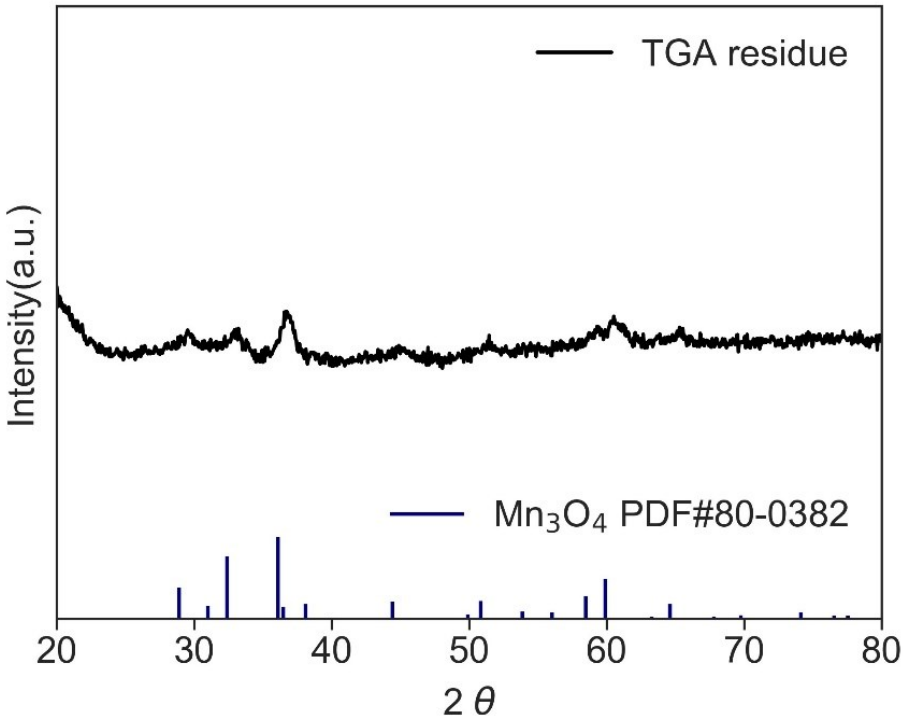

Figure S3. The residue of TGA on MnO@C XRD of is found to be Mn_3O_4.

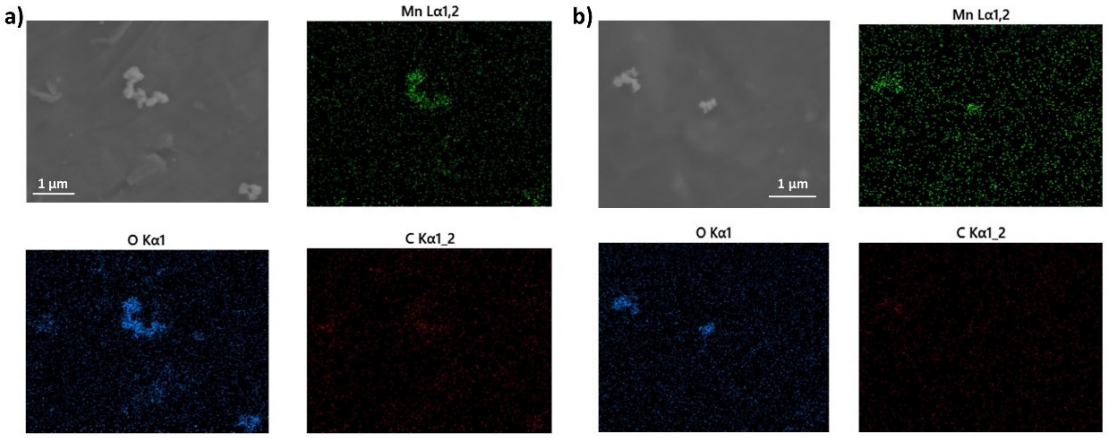

Figure S4. EDS mapping of (a) Mn_3O_4-300 and (b) Mn_2O_3-400.

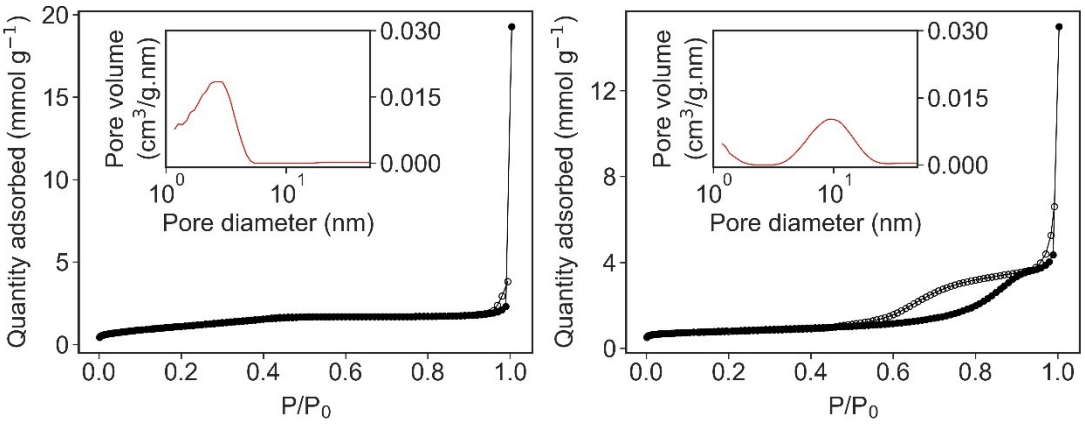

Figure S5. The N_2 isotherm and DFT pore distribution of (a) Mn_3O_4-300 and (b) Mn_2O_3-400, respectively.

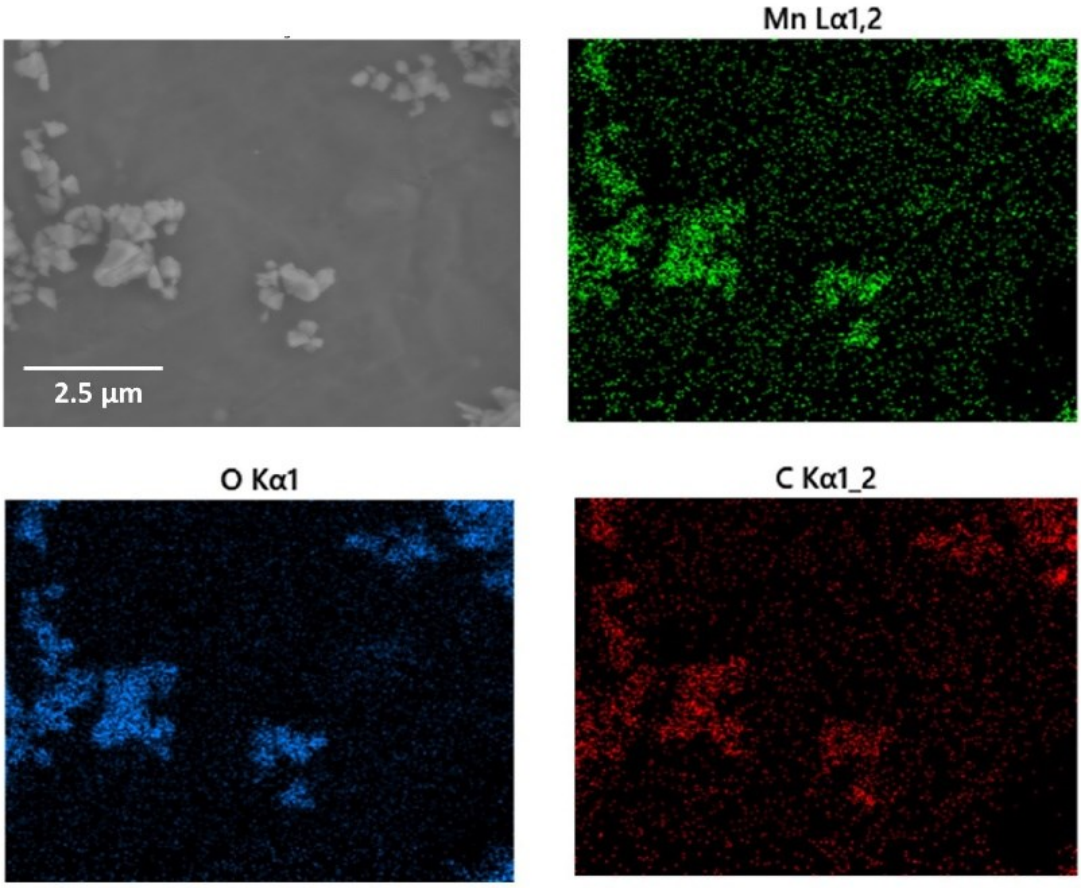

Figure S6. EDS mapping of Mn_3O_4@C-5h.

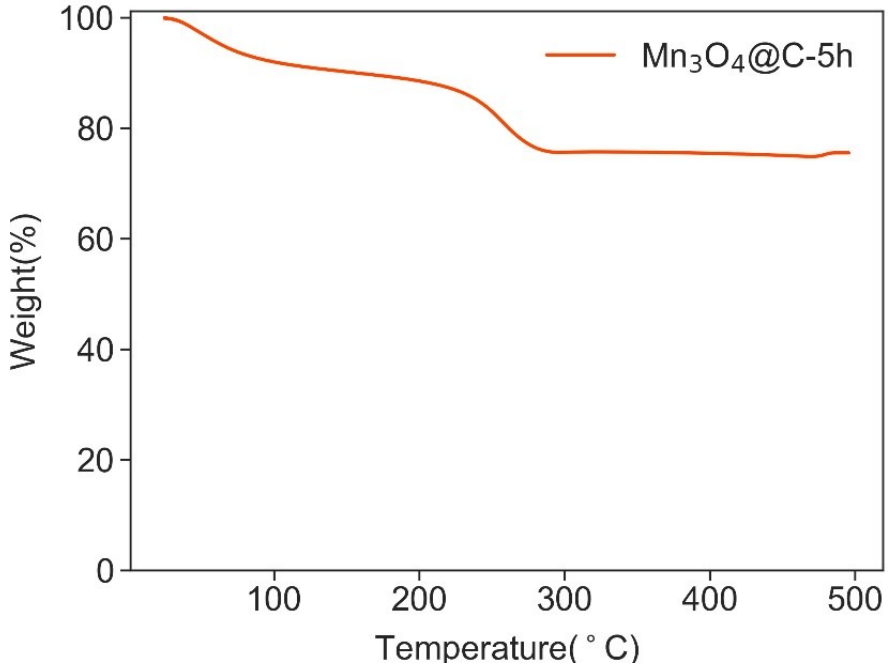

Figure S7. The TGA result of Mn_3O_4@C-5h.

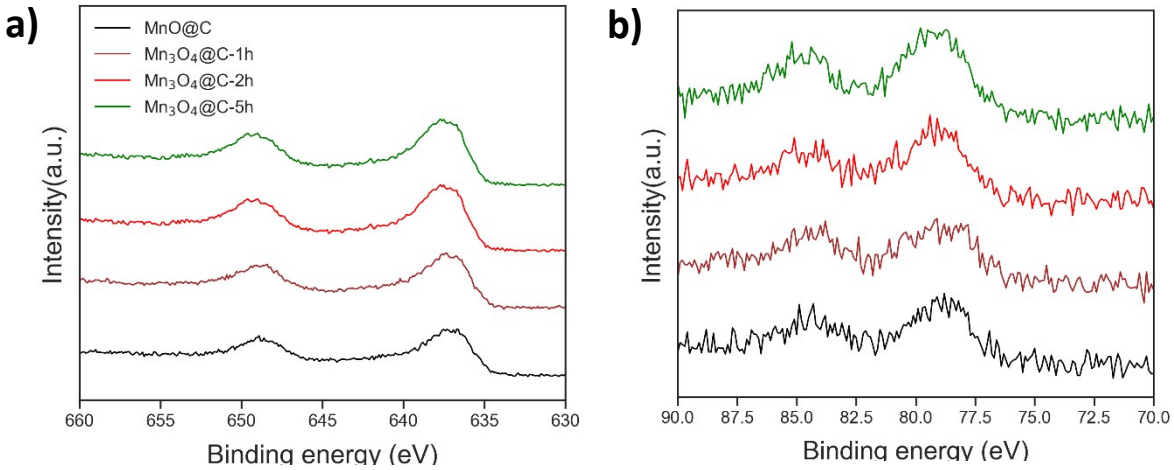

Figure S8. XPS spectroscopy for a) Mn 2p, and b) Mn 3s.

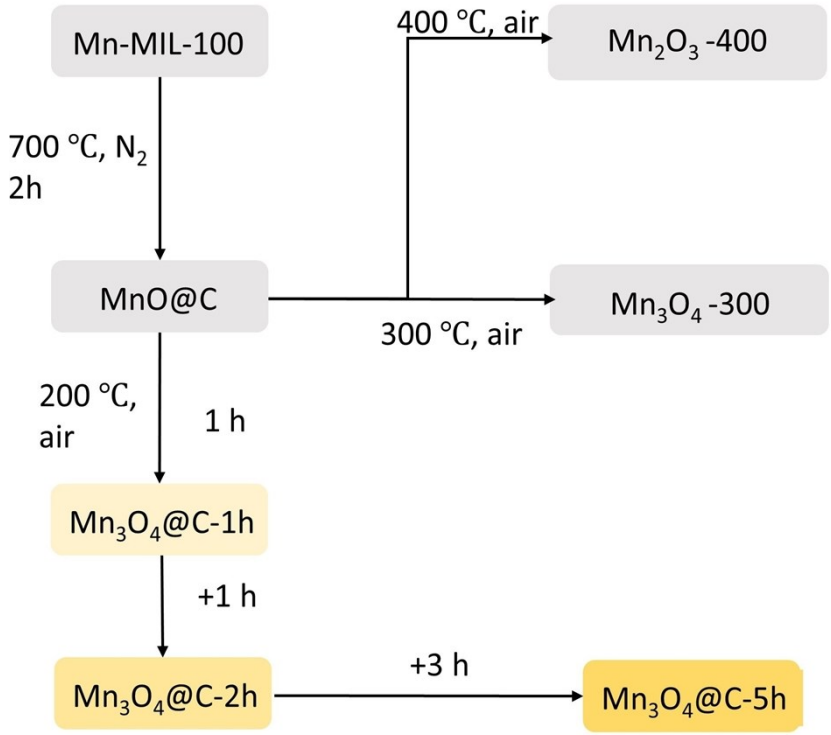

Figure S9. A summary on the thermolysis processes and their respective products involved in this chapter.

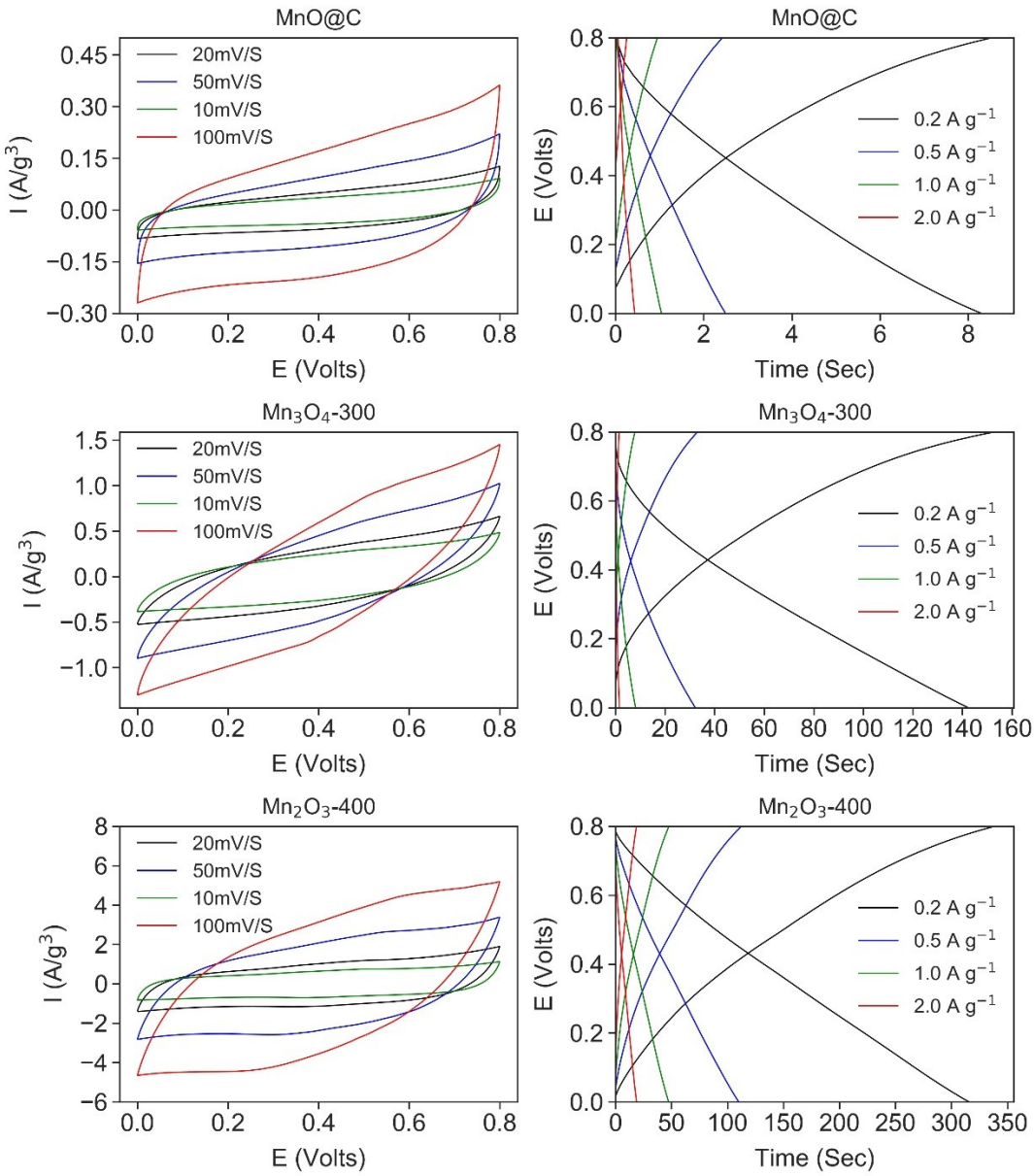

Figure S10. The CV and GCD patterns of MnO@C, Mn_3O_4-300 and Mn_2O_3-400, respectively.

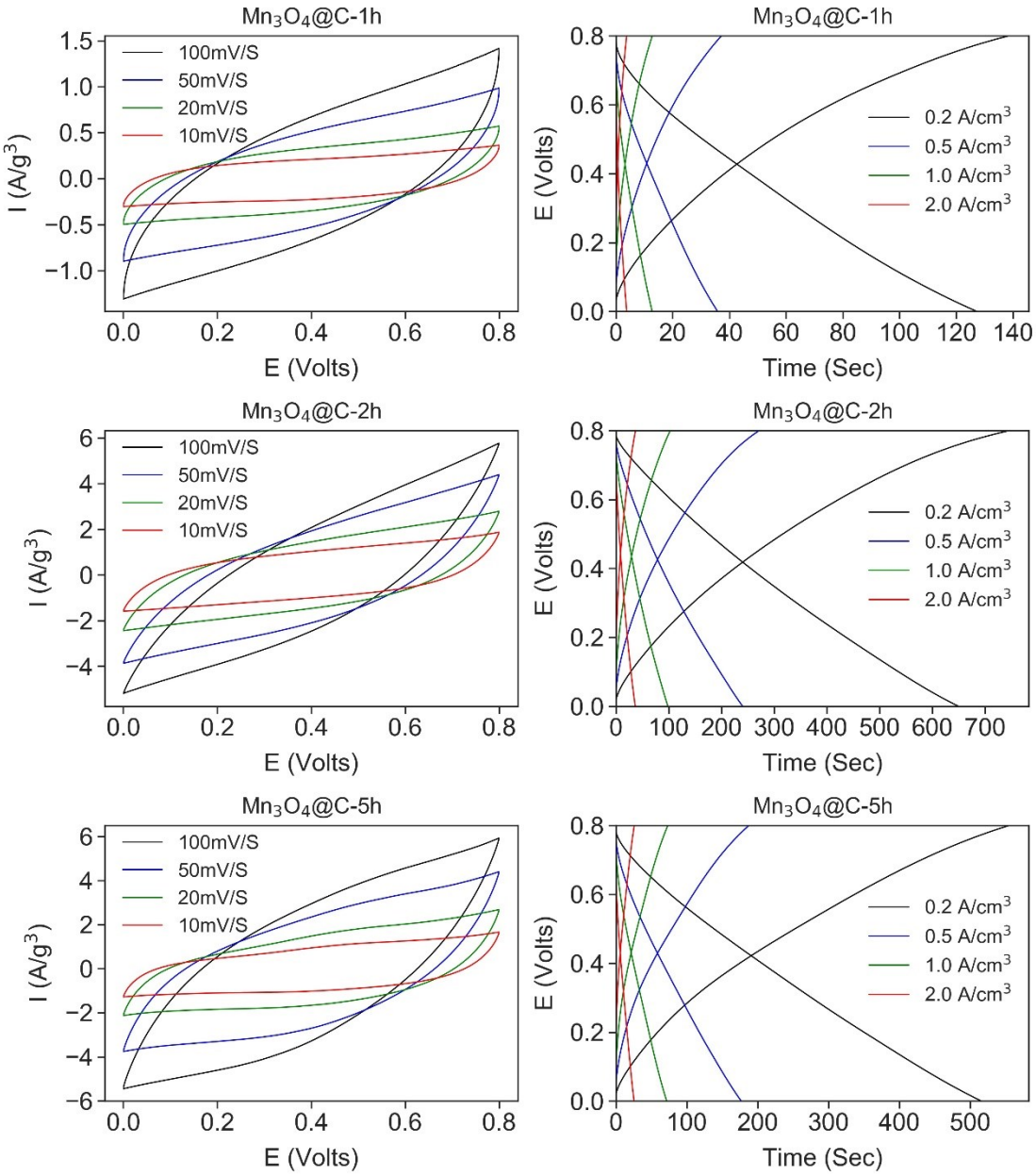

Figure S11. The CV and GCD patterns of Mn_3O_4@C-1h, Mn_3O_4@C-2h and Mn_3O_4@C-5h, respectively.

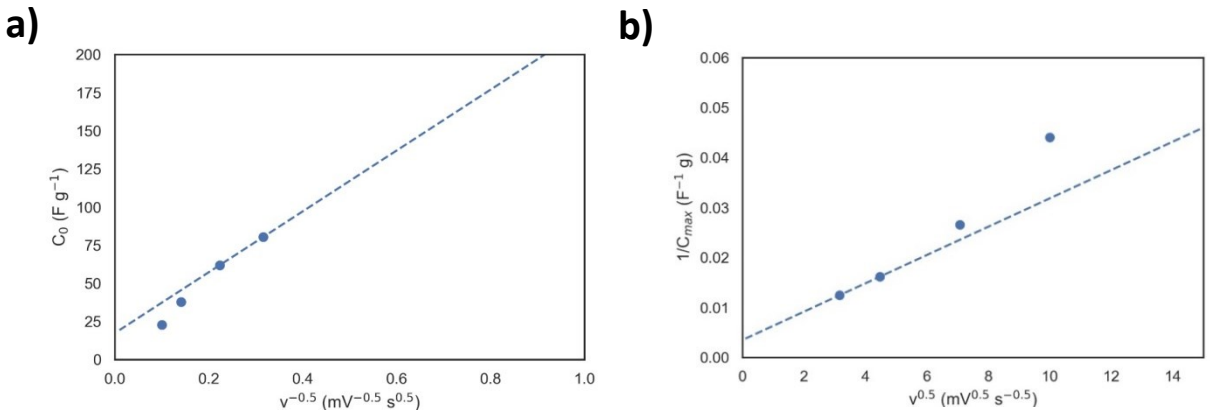

Figure S12. (a) double-layer capacitance C_0, and (b) maximum capacitance C_{max} of Mn_3O_4@C-2h.

The double-layer capacitance C_0 and maximum capacitance C_{max} of Mn_3O_4@C-2h. were estimated to be 17.3 F g^{-1} and 285.7 F g^{-1} respectively, by the Trassatti's method. The relative contribution of double-layer capacitance was thus within the region of ~10 % (6.1 %). It is worth nothing that we only selected the two low frequency (i.e., v = 10 mV/s and 20 mV/s) data points from the available data due to the obvious deviation from linear relationship when the scan rate increases as a result of the internal resistance.

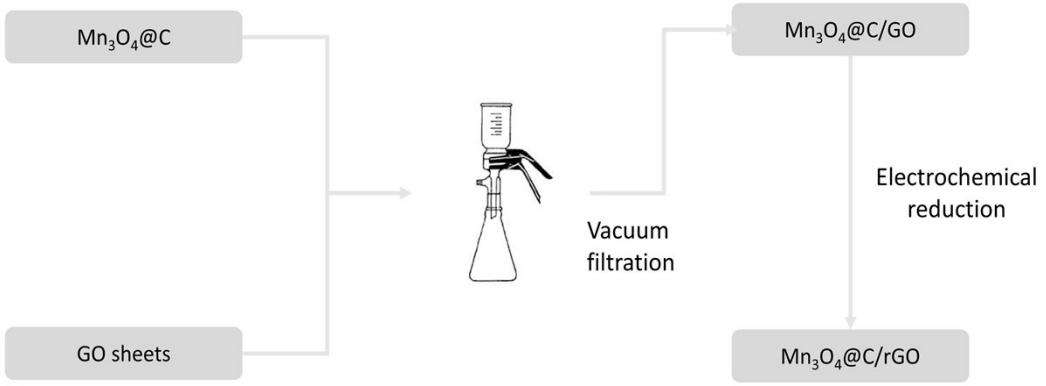

Figure S13. Schematic illustrating the manufacturing process of Mn_3O_4@C/rGO electrode.

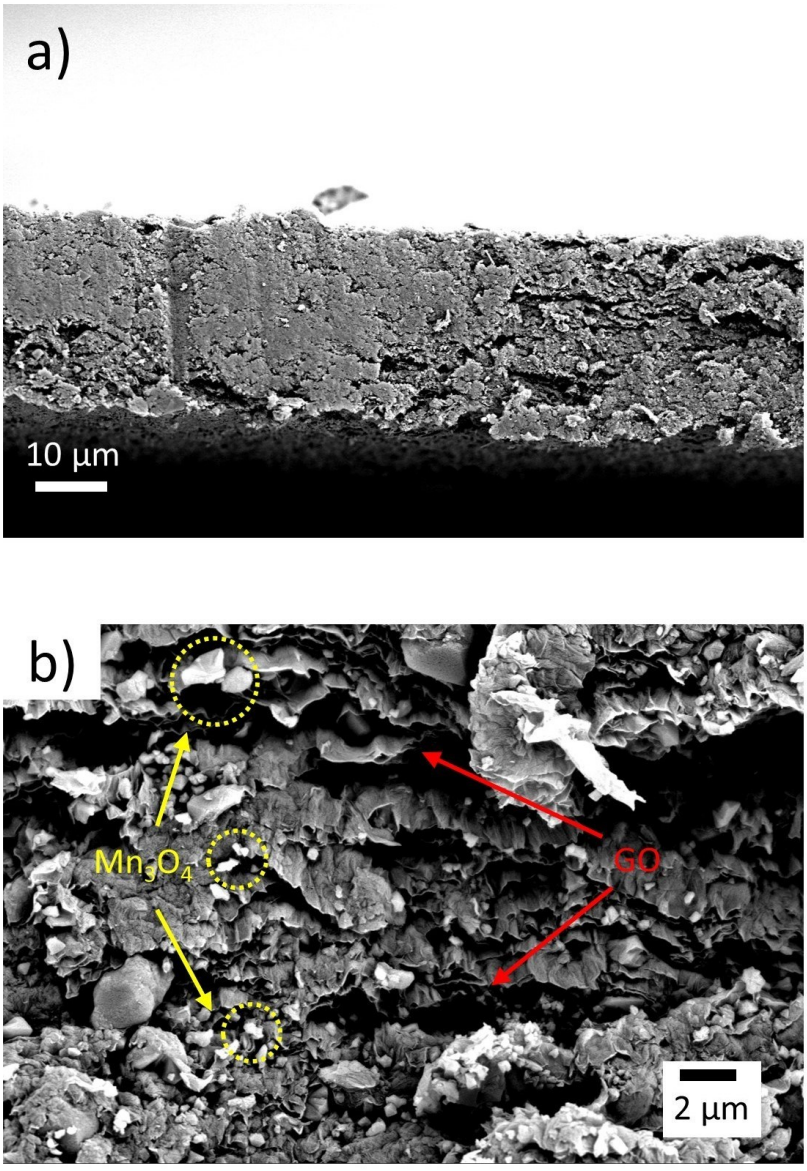

Figure S14. The cross-section SEM of Mn_3O_4@C/GO.

Figure S15. The demonstration of the flexibility of Mn_3O_4@C/GO.

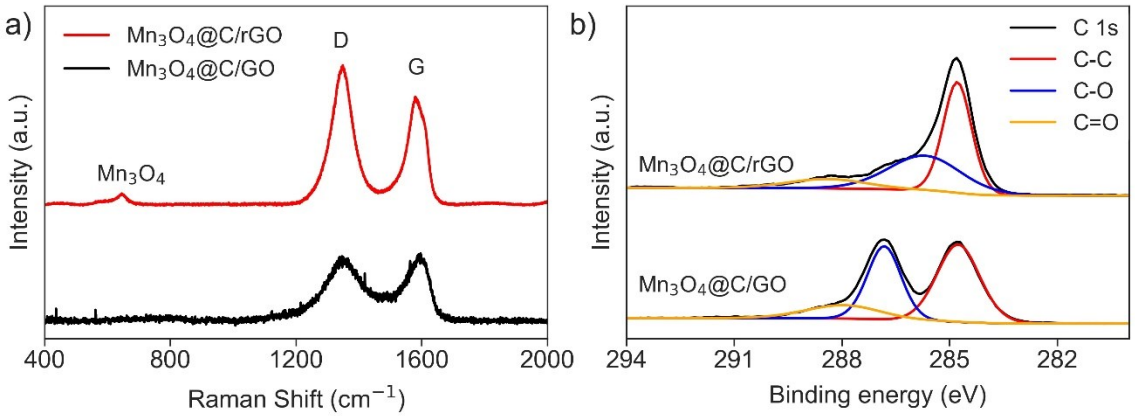

Figure S16. (a) Raman and (b) XPS analysis results of Mn_3O_4@C/GO and Mn_3O_4@C/rGO.

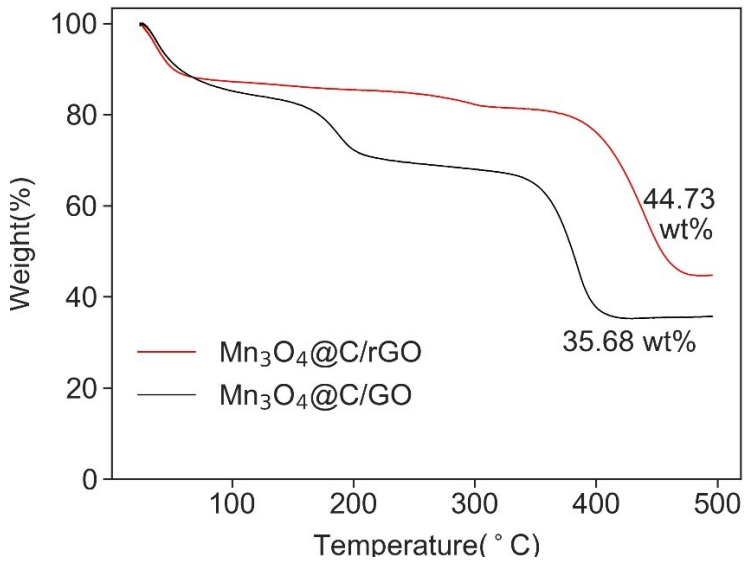

Figure S17. The TGA results of Mn_3O_4@C/GO and Mn_3O_4@C/rGO, respectively.

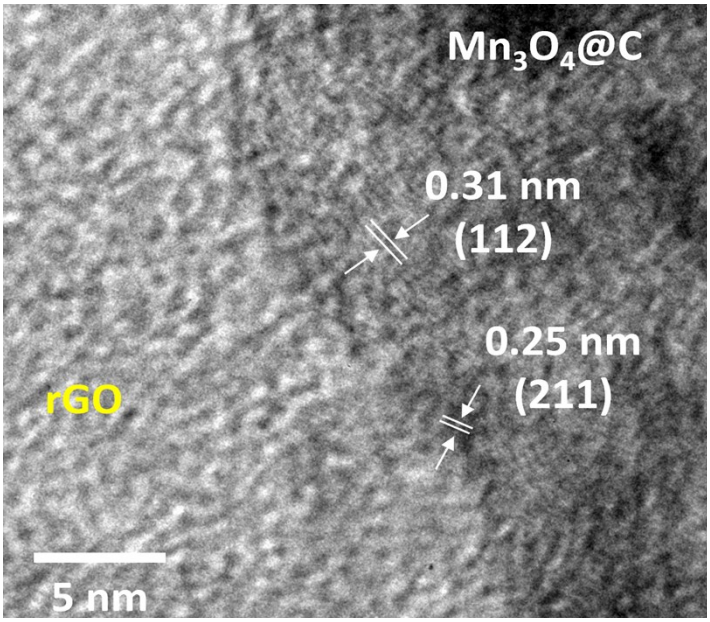

Figure S18. TEM of the Mn_3O_4@C/rGO.

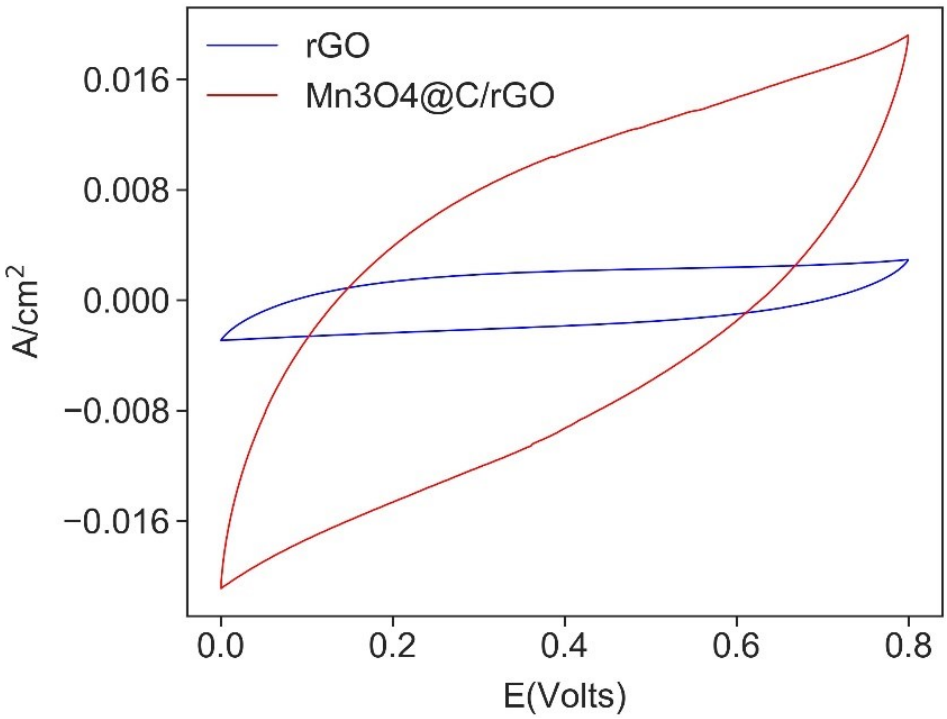

Figure S19. The CV pattern of Mn_3O_4@C/rGO and rGO.

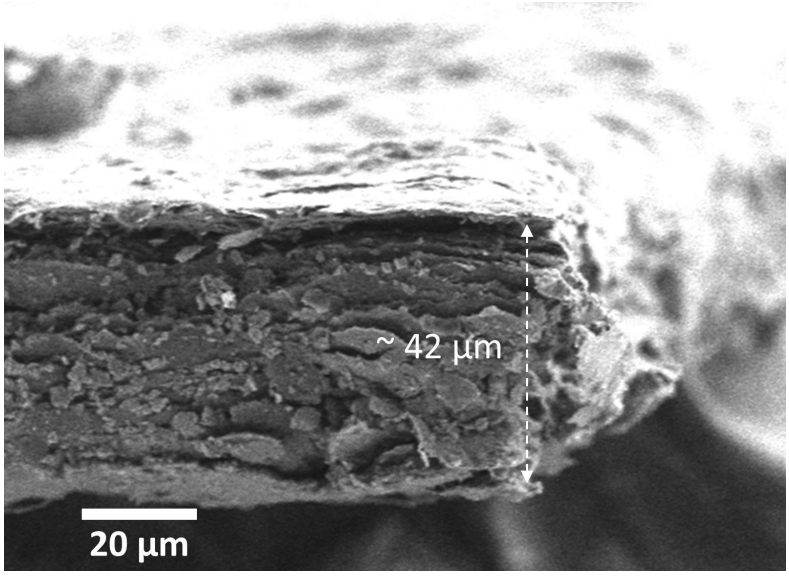

Figure S20. The cross-section SEM of CNT/rGO.

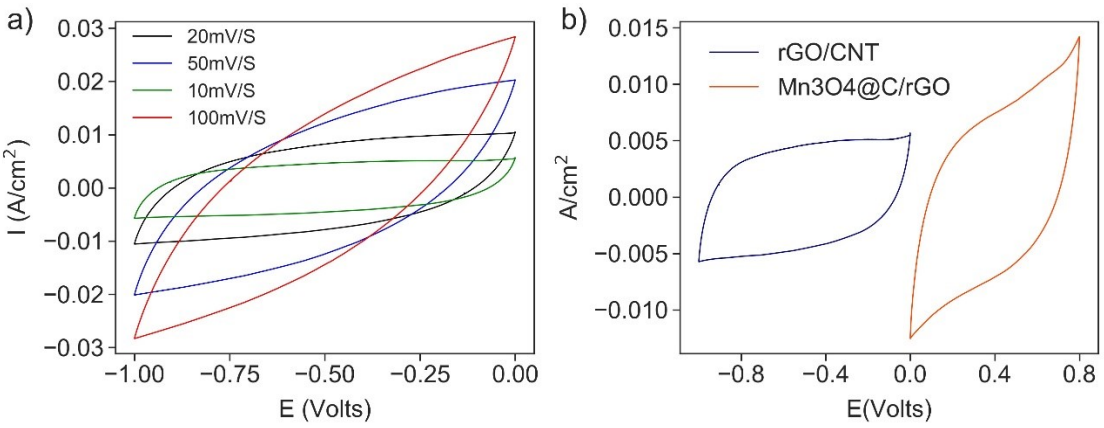

Figure S21. (a) CV patterns of the CNT/rGO paper electrode. (b) CV curves of CNT/rGO and Mn_3O_4@C/rGO, respectively, at 10 mV/s.